The catalytic process of poly-silicate-ferric (PSF) and generation mechanism of hydroxyl radical based on photo-Fenton system

Zhiqing Liu, Jianxin Chen, Jianxi Zhu, Lizhang Liu and Zili Jiang

ABSTRACT

Poly-silicate-ferric (PSF) was developed as an heterogeneous UV-Fenton catalyst, which was characterized by Fourier transform infrared (FTIR) spectroscopy, X-ray diffraction (XRD), X-ray photoelectron spectroscopy (XPS), X-ray fluorescence (XRF), UV-vis diffuse reflectance spectroscopy (DRS), Brunauer–Emmett–Teller (BET) and scanning electron microscopy (SEM). The catalytic process of PSF and generation mechanism of hydroxyl radical based on photo-Fenton system were studied in detail. In the heterogeneous UV-Fenton system, the k_{app} value of Orange II degradation was as high as 0.268 min^{-1}, which was 1.5 times compared to that with α-FeOOH as catalyst. As a result, the Orange II decolouration and mineralization rates were as high as 99.9% and 92.5% after 40 min treatment, respectively. Moreover, the hydroxyl radical concentration would increase to a peak value of 13.4 μmol/L at about 15 min. The fundamental cause of the high hydroxyl radical generation lay in the high release ability of iron ions from PSF. The peak concentrations of total iron ions and ferrous ions could increase to 4.53 mg/L and 1.57 mg/L at 20 min and 10 min, respectively. After treatment, the re-adsorption of iron ions on the surface of PSF could avoid the additional pollution caused by iron ions. The results confirmed that PSF was a high activity catalyst for an heterogeneous UV-Fenton system.

Key words | degradation, hydroxyl radical, iron ions, Orange II, poly-silicate-ferric, UV-Fenton

Zhiqing Liu
Jianxin Chen (corresponding author)
Zili Jiang
Key Laboratory of Poyang Lake Environment and Resource Utilization, Ministry of Education, School of Resources Environmental & Chemical Engineering,
Nanchang University,
Nanchang 330031, Jiangxi,
China
E-mail: *jxchen@ncu.edu.cn*

Jianxi Zhu
Guangzhou Institute of Geochemistry, Chinese Academy of Sciences (CAS),
Guangzhou 510640, Guangdong,
China
and
Guangdong Provincial Key Laboratory of Mineral Physics and Materials,
Guangzhou 510640, Guangdong,
China

Lizhang Liu
Jiangxi Academy of Environmental Sciences,
Nanchang 330077, Jiangxi,
China

INTRODUCTION

Recently, advanced oxidation technology has attracted attention as an effective treatment technology for industrial organic wastewater (Karci *et al.* 2013; do Nascimento *et al.* 2018). UV-Fenton technology is widely studied for treatment of printing and dyeing wastewater because of its high degradation efficiency and easy operation (Yang *et al.* 2018). In general, this technology can be divided into two basic types: homogeneous and heterogeneous UV-Fenton oxidation processes (De La Cruz *et al.* 2012; Guo *et al.* 2015). The homogeneous UV-Fenton system has high degradation efficiency but suffers from secondary pollution of iron ions catalysts after treatment (Wang *et al.* 2015; Yu *et al.* 2016; Qian *et al.* 2017; Leifeld *et al.* 2018). On the contrary, in heterogeneous UV-Fenton system, the solid catalysts-loaded iron ions can be reused but suffer from low catalytic efficiency during organic wastewater treatment (Chen & Zhu 2011).

According to the latest study, both homogeneous and heterogeneous UV-Fenton processes could be detected even if the stable iron oxides are used as heterogeneous catalysts (Kakavandi *et al.* 2016; Wang *et al.* 2016; Huang *et al.* 2017). In these systems, iron ions would leach and go back to the surface of iron oxides during organic pollutants' degradation. As a result, the catalysts of iron oxides acted as not only source but also sink of iron ions (Miao *et al.* 2018). For heterogeneous UV-Fenton system, a conclusion could be made that the ideal catalytic process should take full advantages of homogeneous reactions for organic pollutant degradation and heterogeneous catalyst for reuse after treatment. Unfortunately, the iron leaching process was usually inhibited by the high stability of iron oxides although they were considered as good catalysts for heterogeneous UV-Fenton system (Kakavandi *et al.* 2016; Miao *et al.* 2018; Rosari & Ardiansyah 2019). And the key for solving this

doi: 10.2166/wst.2020.150

problem may lie in the effective release of iron ions from heterogeneous catalysts. Based on this finding, in our previous work, an enhanced method of catalytic efficiency was studied in heterogeneous UV-Fenton system with Fe_3O_4 or α-FeOOH as catalyst (Dai *et al.* 2018; Miao *et al.* 2018). It was proved that the additional oxalate could increase both iron ions leaching and hydroxyl radical generation (Dai *et al.* 2018; Miao *et al.* 2018). Additional enhanced reagents is an external cause while active component of catalyst is the internal cause for increasing the catalytic activity of catalyst. So, developing a novel catalyst may be a good alternative. And the new heterogeneous catalyst should have the high release ability of iron ions during catalytic process and high adsorption ability for iron ions after treatment.

Poly-silicate-ferric (PSF) is a type of inorganic polymer coagulant which is widely used for effective removal of suspended solids in wastewater (Sun *et al.* 2011; Liu *et al.* 2017). And its synthetic method is simple and feasible on the basis of poly-silicic acid and ferric salts. The stability of Si-Fe-O bond in PSF is lower than that of Fe-O bond in iron oxides. So, it could be deduced that the release ability of iron ions from PSF will be higher than that of iron oxides in heterogeneous UV-Fenton system. Furthermore, PSF has distinct abilities of iron irons adsorption and solid-liquid separation after wastewater treatment. Thus, the application of PSF as catalyst in heterogeneous UV-Fenton system is attractive due to its pretty unique properties and low cost. However, few studies have been carried out to detect this interesting catalyst in heterogeneous UV-Fenton system.

Therefore, in this study, PSF was developed as catalyst in heterogeneous UV-Fenton system. The catalytic performance of PSF was examined in terms of the degradation and mineralization of Orange II. The release and re-adsorption of iron ions as well as the ·OH radical generation was studied in detail. This study will provide novel insight into catalytic process of PSF in heterogeneous UV-Fenton system.

MATERIALS AND METHODS

Chemicals

All chemicals except Orange II were analytical grade. Orange II, coumarin (99%) and 7-hydroxycoumarin (99%) were provided by Aladdin Chemistry Co., Ltd (Shanghai, China) and the other chemicals were purchased from Sinopharm Chemical Reagent Co., Ltd (Shanghai, China).

Synthesis of polymer silicates

The polymer silicates were synthesized according to the literature methods using nitrates and Na_2SiO_3 as precursors (Fu *et al.* 2007; Sun *et al.* 2011). Firstly, the solution of Na_2SiO_3 was added dropwise into nitrate solution at room temperature under magnetic stirring until the pH reached 8.0 ± 0.2. Then the solution mixture was kept for 6 hours at 60 °C. Secondly, the precipitate was collected and washed repeatedly with deionized water until the pH reached 7.0. Finally, the precipitate was dried at 333 K in the oven, then ground grinded over 200 mesh and stored in polyethylene bottles.

Degradation experiment

The catalytic activities of different polymer silicates were evaluated in a photochemical reactor which was described in our previous work (Miao *et al.* 2018). Initial conditions: Orange II concentration was 0.2 mmol/L and the initial pH value was 3.0 adjusted by HCl (Miao *et al.* 2018). The dosage of catalyst and the concentration of H_2O_2 were 1.0 g/L and 10 mmol/L, respectively (Miao *et al.* 2018). Before reaction, the catalyst and Orange II were put into reactor and stirred in dark for 30 min to achieve adsorption equilibrium (Dai *et al.* 2018; Miao *et al.* 2018). Then H_2O_2 was added in solution and the UV-light was turned on to initiate the reaction. At predetermined time intervals, samples were withdrawn and filtered immediately through 0.45 μm filter film (Dai *et al.* 2018; Miao *et al.* 2018).

Analysis methods

The structures of PSF were detected by X-ray diffraction (XRD) and Fourier transform infrared (FTIR) spectroscopy. The chemical composition and state of the sample surface were detected by X-ray photoelectron spectroscopy (XPS). The contents of PSF were determined by X-ray fluorescence (XRF) spectrometer. The specific surface area and pore size distribution were analyzed by a surface area and porosity analyzer. The morphology and particle size of PSF were observed by electron scanning electron microscopy. Its optical response range of the sample was determined by an ultraviolet visible diffused reflection spectrophotometer.

Orange II concentration was determined on a visible spectrophotometer (V1600, AOE instrument Co., China) at wavelength of 484 nm (Dai *et al.* 2018; Miao *et al.* 2018). Hydrogen peroxide concentration was measured using the titanate spectrophotometric method (Dai *et al.* 2018; Miao

et al. 2018). Hydroxyl radical concentration was analyzed quantitatively using coumarin as a fluorescence probe on optical fiber (QE 65Pro, Ocean Optics, USA) (Dai et al. 2018; Miao et al. 2018). Total organic carbon (TOC) of the sample was measured using Multi N/C Analyzer (2100, Analytik Jena) (Dai et al. 2018; Miao et al. 2018). Total dissolved iron concentration was determined by inductively coupled plasma-atomic emission spectrometry (Optima 2100 DV, Perkin Elmer) (Dai et al. 2018; Miao et al. 2018). Ferrous ion concentration was examined according to the 1,10-phenanthroline method (Dai et al. 2018; Miao et al. 2018).

RESULTS AND DISCUSSION

Characterization of PSF

The IR spectra of PSF before and after UV-Fenton reaction are represented in Figure 1. Both spectra exhibited two characteristic bonds at 3,420 cm^{-1} and 1,635 cm^{-1}, which can be attributed to the stretching vibration of -OH and the bending vibration of water (Sun et al. 2011). The peak appearing near 1,383 cm^{-1} was the stretching vibration peak of the -OH group connected to Fe^{3+} (Fu et al. 2009). The peak at 1,012 cm^{-1} could be attributed to absorption vibration of Si-O-Fe bond in PSF (Sun et al. 2010). In addition, the peaks at 776 cm^{-1} and 450 cm^{-1} were related to the stretching vibration of Al-OH bond and the vibration of Fe-O bond, respectively (Li et al. 2017, 2018). The IR analysis confirmed that the PSF was successfully synthesized through the polymerization process. Furthermore, no major change in IR pattern of the catalyst was observed after treatment, which suggested that the catalytic reaction has no effect on the structure of the PSF.

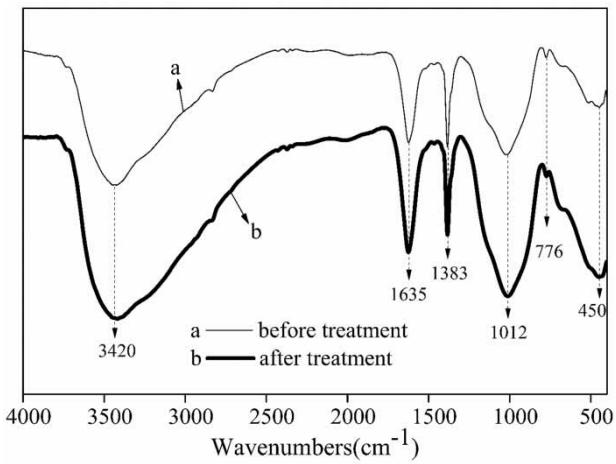

Figure 1 | FTIR spectra of PSF before and after catalytic process.

The phase composition of PSF was characterized by XRD and the result is shown in Figure S1 (Supplementary Material). It could be seen that the diffraction peak of PSF was amorphous, which implied that no standard crystals could be observed in PSF. Similar phenomena were reported by Fu (Fu et al. 2007). Combined with IR spectra, it could be deduced that the PSF was an amorphous material formed by the polymerization of Si, Fe and O. XRF analysis confirmed that the PSF was mainly composed by three kinds of elements: O, Si and Fe (Table S1, Supplementary Material). And these three elements accounted for 99.4% of the components of PSF, indicating high purity of the synthesized catalyst. It was reported that a stable dendritic structure of PSF could be synthesized after a series of changes such as bond breaking and bond recombination. The chemical bonding type of Si-Fe-O bonds was Si-O-Fe-O-Fe-O-Si in PSF when the Si/Fe ratio was low (Fu et al. 2007). In our synthesized catalyst, the element content ratio of Si to Fe was 0.91, which indicated that a similar structure had been obtained.

As shown in Figure 2(a), Fe2p, Si2p and O1s peaks appeared in XPS spectrum of PSF, which also indicated that Si, Fe and O were the main elements on the surface of PSF. It can be seen from Figure 2(a) that the binding energy of the elements contained in the PSF before and after the reaction did not change much, which indicating that the PSF has good stability as catalyst. The high-resolution XPS spectra of Fe2p is shown in Figure 2(b). The peak at 711.8 eV indicated that lots of Fe^{III} existed on the surface of PSF (Su et al. 2019). The binding energy of 710.8 eV was the typical Fe2p peak of Si-O-Fe which was consistent with FTIR results (Zhang et al. 2017). It can be seen from Figure 2(b) that the binding energy of iron has no major change after the reaction, which indicates that iron ions in the solution can be re-adsorbed back to the catalyst surface after the reaction. The high-resolution XPS spectra of O1s is shown in Figure 2(c). The binding energies at 530.4 eV and 532.1 eV were the peak of Fe-O and Fe-O-C, respectively (Su et al. 2019). The binding energy of 531.2 eV and 532.9 eV were the peak of Si-O-Fe and -COOH, the peak of -COOH may be related to the adsorption of intermediate products on the catalyst (Ali et al. 2018). The high-resolution XPS spectra of C1 s is shown in Figure 2(d). The binding energies at 284.6 eV and 285.8 eV were the peak of C-C and C-O (Shuai et al. 2018), respectively. The binding energies at 288.5 eV was the peak of -COOH, which may be related to the

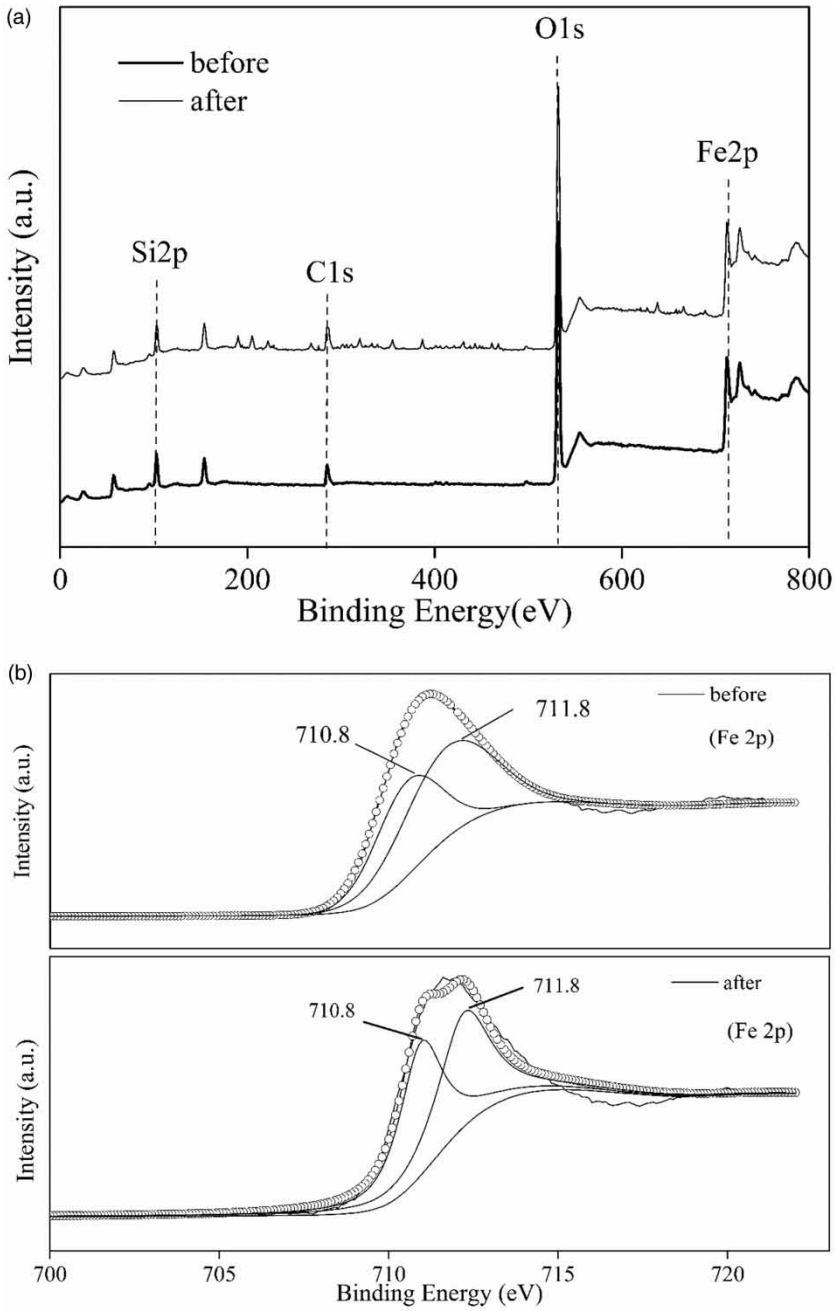

Figure 2 | XPS spectra of PSF before and after reaction: (a) the full survey spectra analysis of PSF; (b) the high-resolution XPS spectra of Fe2p; (c) the high-resolution XPS spectra of O1s; (d) the high-resolution XPS spectra of C1s. *(Continued.)*

intermediate products being adsorbed on the catalyst (Shuai *et al.* 2018).

The UV-vis DRS absorption spectra of PSF is shown in Figure S2. The $(Ahv)^{1/2} \sim hv$ relationship curve was obtained according to the Tauc rule (Li *et al.* 2019). The linear portion of the curve was extended to intersect the axis of abscissa, and the abscissa of the intersection could be estimated to be 1.64 eV. The results showed that PSF could effectively absorb light in the range of 200–600 nm because of the surface Fe^{III}.

The surface roughness of PSF was detected by SEM shown in Figure 3. The SEM photograph shows that the synthetic PSF was a block structure of micron grade (Figure 3(a)) and relatively rough (Figure 3(b)). Based on N_2 adsorption/desorption curve (Figure S3), the external and micropore surface area were measured to be

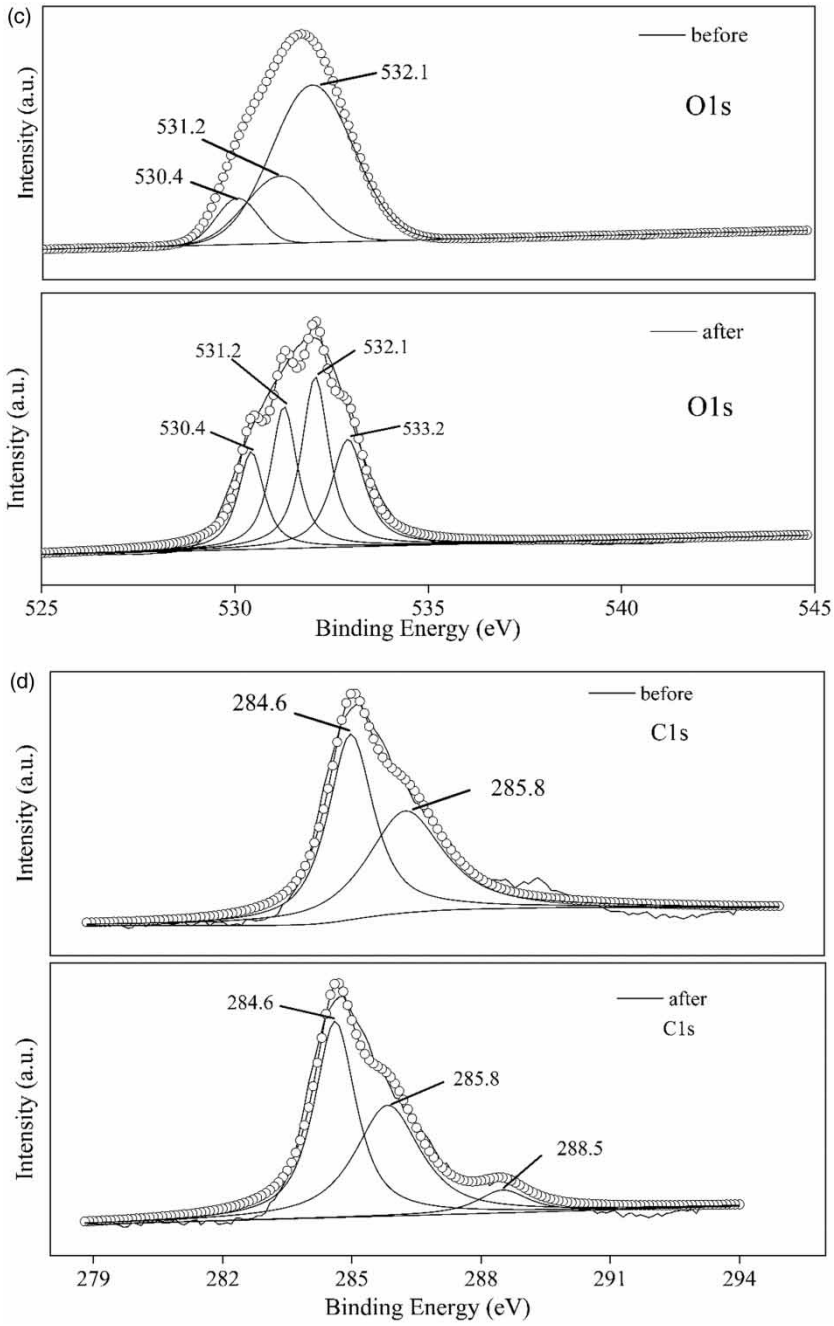

Figure 2 | Continued.

127.24 m^2/g and 153.13 m^2/g, respectively. The high external surface area of PSF could provide more catalytic active sites for hydroxyl radical generation.

Catalytic activity of PSF

The decolouration of Orange II under different reaction conditions is shown in Figure 4(a). The corresponding pseudo-first-order rate constants are shown in Figure S4. The major cause of Orange II decolouration is the break of nitrogen double bonds (Chen *et al.* 2011). As shown in Figure S4, the rate constant (k_{app}) values in UV and UV-H_2O_2 systems were 0.003 min^{-1} and 0.109 min^{-1}, respectively. In UV-H_2O_2 system, hydroxyl radicals could be produced by photolytic split of H_2O_2 (Equation (1)) and 95.3% of decolouration rate was obtained within 30 min

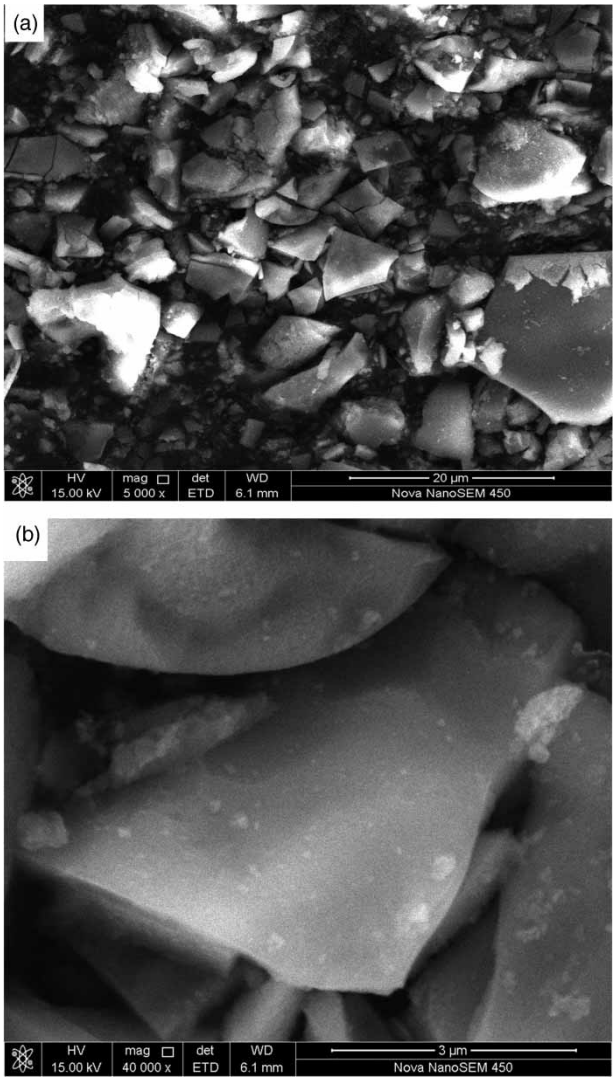

Figure 3 | SEM picture of PSF: (a) the scan of the PSF at 5000 times and (b) the scan of the PSF at 40,000 times.

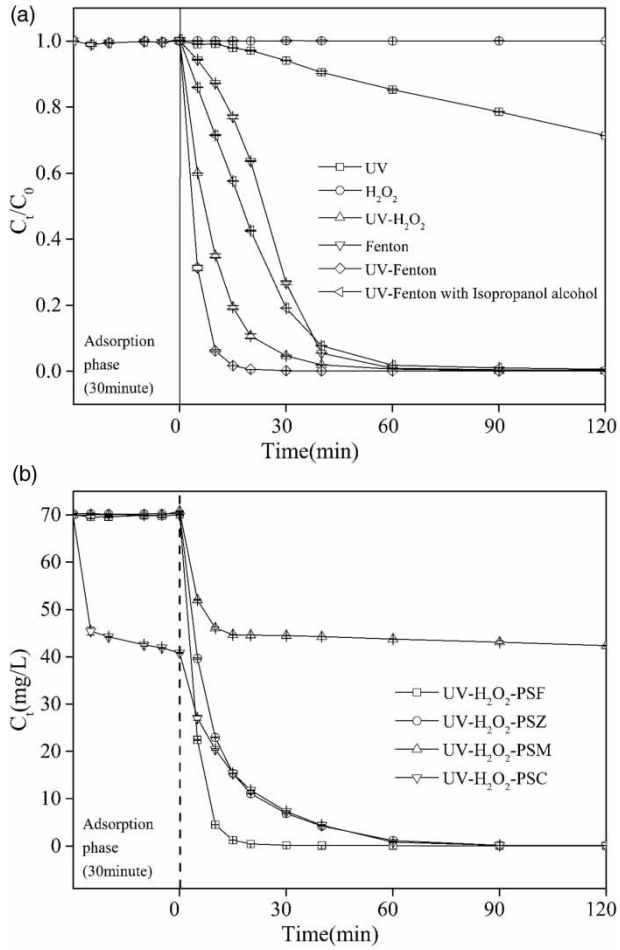

Figure 4 | (a) Decolouration of Orange II under different conditions. (b) Decolouration of Orange II in UV-Fenton systems with different polymer silicates as catalysts.

(Figure 4(a)). So the conclusion could be made that oxidation by hydroxyl radical was more effective than direct photolysis under UV irradiation for Orange II decolouration.

$$H_2O_2 + h\nu \rightarrow \cdot OH + \cdot OH \quad (1)$$

As expected, the fastest Orange II decolouration was obtained in UV-PSF-H_2O_2 system. And 99.4% of decolouration rate was obtained within 20 min (Figure 4(a)). Its k_{app} value increased to 0.268 min^{-1}, which was 2.5 times as high as that in UV-H_2O_2 system (Figure S4). The results indicated that PSF was a high activity catalyst for hydroxyl radicals generation in UV-Fenton system. The conclusion was confirmed by a scavenging experiment given in Figure 4(a). The results showed that the Orange II decolouration rate decreased from 99.4% to 58.4% at 20 min and the k_{app} value decreased from 0.268 min^{-1} to 0.033 min^{-1} when isopropyl alcohol was added. Since isopropyl alcohol was considered as efficient scavenger for hydroxyl radical, the results proved that hydroxyl radical was the main active oxidation species for Orange II decolouration.

Under UV irradiation, the catalytic activities of different polymer silicates (poly-silicic-manganese: PSM; poly-silicic-copper: PSC; poly-silicic-zinc: PSZ and poly-silicic-ferric: PSF) on H_2O_2 were detected and shown in Figure 4(b). Accordingly, the pseudo-first-order kinetic fitting for Orange II decolouration is presented in Figure S5. The decolouration rate constants of Orange II were 0.057 min^{-1}, 0.059 min^{-1}, 0.113 min^{-1} and 0.268 min^{-1} when the catalysts were PSM, PSC, PSZ and PSF, respectively. It should be noted

that only PSF showed high efficiency catalytic ability compared to the decolouration rate constant of Orange II in UV-H_2O_2 system.

Based on our previous experimental results of different iron oxides (Xu *et al.* 2017; Dai *et al.* 2018; Miao *et al.* 2018), the catalytic ability of PSF for Orange II degradation in heterogeneous UV-Fenton system was analyzed and compared, and the results are shown in Table 1. It could be seen that the catalytic ability of PSF was significantly higher than that of iron oxides. Compared with α-FeOOH (the highest catalytic ability among iron oxides), the increasing rate of catalytic ability of PSF reached 51%.

The mineralization of Orange II in UV-Fenton system

Generally, the visible absorption peak of Orange II at 484 nm was due to characteristic bands of nitrogen double bonds (Moon *et al.* 2011; Chen *et al.* 2012; Zulfiqar *et al.* 2018). The ultraviolet absorption peak of Orange II at 310 nm was the characteristic absorption of the naphthalene rings (Paz *et al.* 2018; Tan *et al.* 2018). So the decrease of absorption peaks at 484 nm and 310 nm could be ascribed to the degradation of nitrogen double bonds and naphthalene rings, respectively. Once the nitrogen double bonds of Orange II broke, the dye decolouration would occur.

To detect the degradation of Orange II in Fenton and UV-Fenton systems, the UV-vis spectral changes of Orange II and the TOC concentrations as a function of irradiation time were studied and shown in Figure 5. It was clear that the absorption peak at 484 nm decreased faster than that at 310 nm both in Fenton and UV-Fenton systems. The results indicated that the azo-bonds were more active site for oxidative attack of hydroxyl radical. In Fenton system, 53.8% of TOC was removed while complete decolouration was achieved after 120 min treatment. In UV-Fenton system, the Orange II decolouration and mineralization rates were as high as 99.94% and 92.5% after 40 min treatment, respectively. It could be deduced that the concentration of hydroxyl radical generated in UV-Fenton system was higher than that in Fenton system. And the results confirmed that PSF was a high activity catalyst for Orange II mineralization in UV-Fenton system.

The catalytic process of PSF and generation mechanism of hydroxyl radical

In scavenging experiment (shown in Figure 4(a)), it was proved indirectly that the hydroxyl radical was the main oxidant for Orange II degradation. As the high reactive radical (•OH) was generated through catalytic decomposition of hydrogen peroxide, the generation of hydroxyl radical would be accordance with the decomposition of hydrogen peroxide. To provide a direct insight into catalytic process of PSF, the leaching of iron ions and decomposition of hydrogen peroxide were detected and shown in Figure 6(a) and 6(b), respectively. Based on fluorescence intensity changes of 7-hydroxycoumarin (Figure S6), the concentrations of hydroxyl radical in different systems were measured and illustrated in Figure 6(b).

In Fenton system, it could be seen that the concentration of total iron ions increased as high as 14.74 mg/L after 120 min reaction (Figure 6(a)). As only 53.8% of TOC could be removed after 120 min treatment, some colorless organic acids would be generated during Orange II degradation (Chen & Zhu 2009). The complex ability of these organic acids with Fe^{III} was so high that the iron leaching from PSF could be promoted. Similar phenomenon was also reported in our previous study (Chen & Zhu 2009). The iron ions were present as Fe^{III}-organic complexes, so the homogeneous Fenton-like reaction (Equation (2))

Table 1 | Pseudo-first-order rate constants of Orange II degradation in heterogeneous UV-Fenton system with different catalysts

Catalyst	Dosage (g/L)	C_{H2O2} (mmol/L)	pH	light resource (nm)	k (min^{-1})	R^2	References
Fe_2O_3	1.0	10	3	254	0.085	0.998	Xu *et al.* (2017)
Fe_3O_4	1.0	10	3	254	0.112	0.997	Xu *et al.* (2017)
α-FeOOH	1.0	10	3	254	0.178	0.955	Miao *et al.* (2018)
Fe_2O_3@ Fe_3O_4	1.0	10	3	254	0.135	0.998	Dai *et al.* (2018)
PSC	1.0	10	3	254	0.059	0.989	This study
PSM	1.0	10	3	254	0.057	0.995	This study
PSZ	1.0	10	3	254	0.113	0.999	This study
PSF	1.0	10	3	254	0.268	0.994	This study

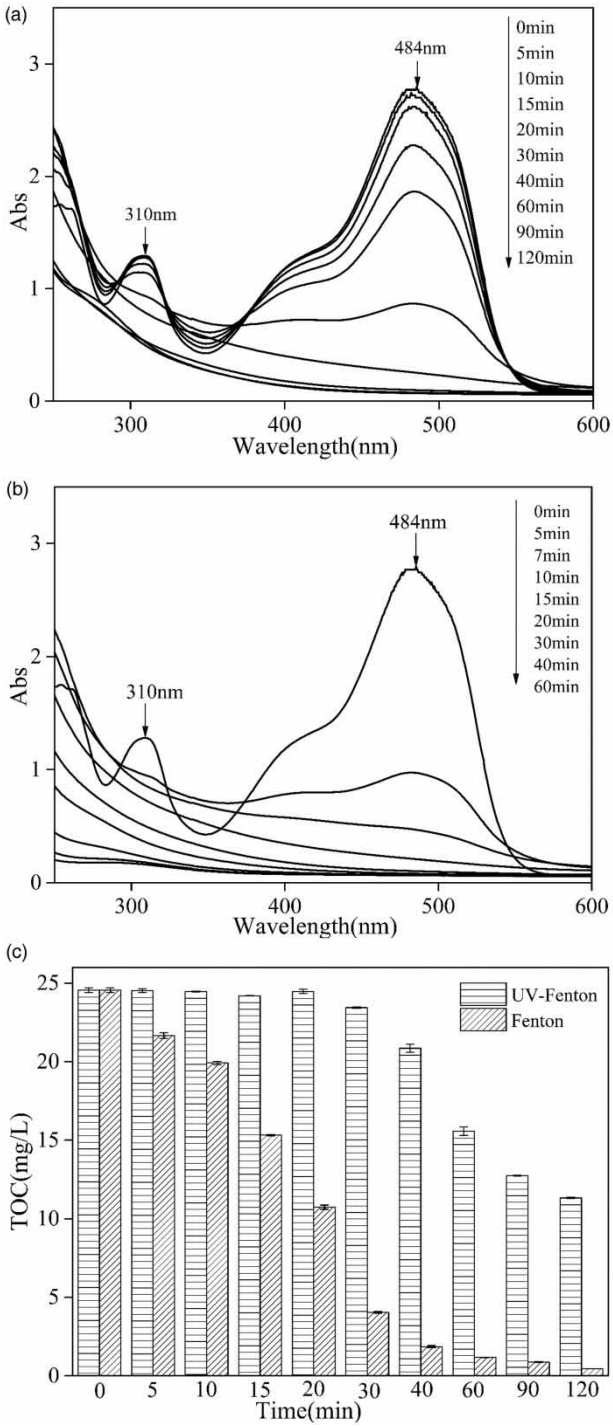

Figure 5 | (a) UV-vis spectral changes of Orange II in heterogeneous Fenton. (b) UV-Fenton systems with PSF as catalyst. (c) The mineralization of Orange II in heterogeneous Fenton and UV-Fenton systems.

between Fe^{III} (aq) and H_2O_2 in solution was hindered (Miao *et al.* 2018). Since the ferrous ions (Fe^{II}) were generated by Fenton-like reaction, the peak concentration of ferrous ions in Fenton system was as low as about 1.17 mg/L at 40 min (Figure 6(a)). As a result, the decomposition of hydrogen peroxide was lowest and the concentration of residual hydrogen peroxide was 3.24 mmol/L after 120 min reaction (Figure 6(b)). Accordingly, the concentration of hydroxyl radical increased slowly and reached a peak values (around 4.2 μmol/L) at about 60 min, then decreased to around 1.13 μmol/L after 120 min reaction. The results indicated that the low concentration of hydroxyl radical was the main reason for the low removal of TOC in Fenton system.

$$Fe^{III}(aq) + H_2O_2 \rightarrow Fe^{II}(aq) + \bullet OOH + H^+ \quad (2)$$

In UV-Fenton system, the concentration of total iron ions increased firstly and reached peak values (around 4.53 mg/L) at about 20 min, then decreased to around 2.13 mg/L after 120 min reaction (Figure 6(a)). On the one hand, the $\equiv Fe^{III}$ on the surface of PSF would be converted into $\equiv Fe^{II}$ under UV irradiation. Then the $\equiv Fe^{II}$ would be released effectively as Fe^{II}(aq) from PSF through the ionic exchange with H^+ in acidic condition. On the other hand, since the residual TOC was around 10 mg/L in UV-Fenton system at 20 min (Figure 5(c)), it could be deduced that total iron ions were partly present as Fe^{III}-organic complexes in solution. Under UV irradiation, the Fe^{III}-organic complexes could be converted to Fe^{II}(aq) through photoreduction pathway (Miao *et al.* 2018). As a results, the peak concentration of Fe^{II}(aq) was about 1.57 mg/L at about 10 min (Figure 6(a)). Then the homogeneous Fenton reaction between Fe^{II}(aq) and hydrogen peroxide occurred (Equation (3)) (Barhoumi *et al.* 2016). The Fenton reaction rate was so fast that the decomposition of hydrogen peroxide could be promoted and the concentration of residual hydrogen peroxide decreased to 0 mmol/L after 120 min reaction (Figure 6(b)). Therefore, the concentration of hydroxyl radical increased fast and reached a peak values (around 13.4 μmol/L) at about 15 min, then decreased to around 0.42 μmol/L after 120 min reaction. This results corresponded to the changes of TOC in solution (Figure 5(c)).

As expected, the peak concentration of hydroxyl radical decreased to 4.7 μmol/L when isopropyl alcohol was added as efficient hydroxyl radical scavenger in UV-Fenton system. In this system, the reaction between H_2O_2 and hydroxyl radical (Equations (4) and (5)) (Guo *et al.* 2014) was limited by the concentration of hydroxyl radical, so the decomposition

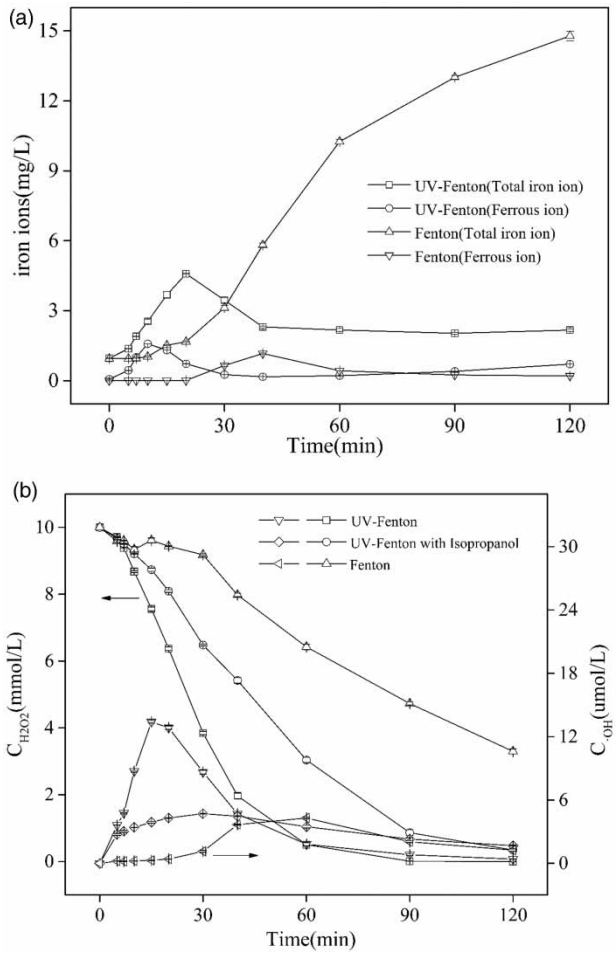

Figure 6 | Concentration of iron ions, hydroxyl radical and hydrogen peroxide as a function of irradiation time in different systems.

rate of hydrogen peroxide decreased.

$$Fe^{II}(aq) + H_2O_2 \rightarrow Fe^{III}(aq) + \bullet OH + OH^- \quad (3)$$

$$H_2O_2 + \cdot OH \rightarrow H_2O + HOO\cdot \quad (4)$$

$$HOO\cdot + \cdot OH \rightarrow H_2O + O_2 \quad (5)$$

As the ion exchange ability is in the order of $Fe^{III}(aq) > H^+ > Fe^{II}(aq)$, the $Fe^{III}(aq)$ generated from Fenton reaction (Equation (3)) could go back to the surface of PSF through the re-adsorption process. The catalytic process of PSF and generation mechanism of hydroxyl radical are summarized in the Figure 7.

According to the EEC regulations, the iron concentrations in wastewater and drinking water must not exceed 5 and 2 mg/L, respectively (Lenoble *et al.* 2005). The results indicated that the additional pollution caused by iron ions could be avoided in UV-Fenton system when PSF was used as catalyst, which was quite different to its Fenton system.

CONCLUSION

In UV-Fenton system, PSF has an advantage over the other polymer silicates in degradation of Orange II. Moreover, PSF has higher catalytic activity than iron oxides in UV-Fenton system. The scavenging experiment proved that hydroxyl radical was the main active species for Orange II decolouration in this system. During the catalytic process,

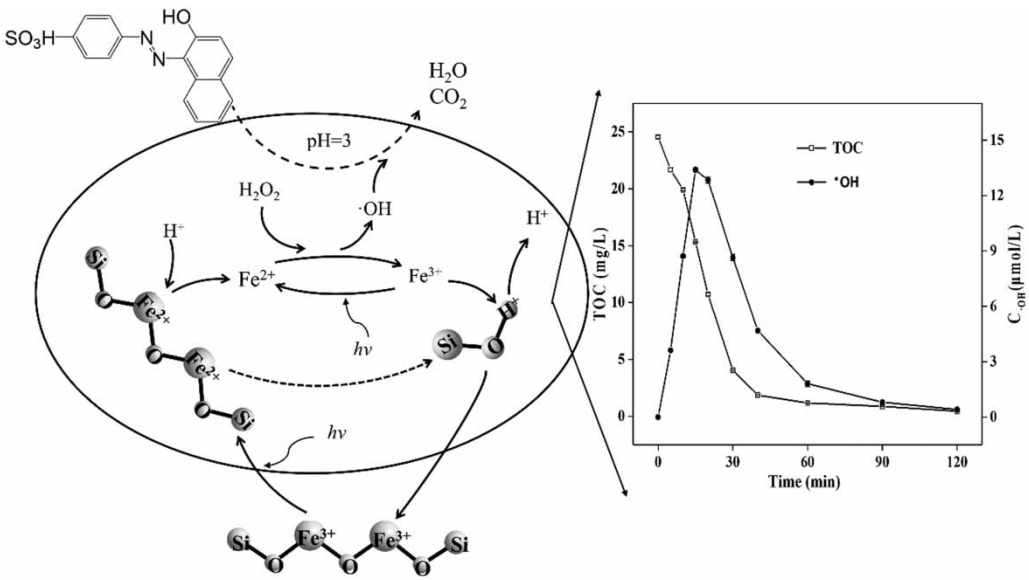

Figure 7 | The catalytic process of PSF and generation mechanism of hydroxyl radical.

the effective release of iron ions from PSF could promote hydroxyl radical generation and Orange II degradation. After treatment, the re-adsorption of iron ions on PSF could avoid the additional pollution caused by iron ions. The results confirmed that PSF was a high activity catalyst for UV-Fenton system.

ACKNOWLEDGEMENTS

We would like to thank the National Natural Science Foundation of China (21966021, 21367021), the Education Department of Jiangxi Province of China (GJJ13072) and Science Technology Planning Project of Guangdong Province of China (2017B030314175) for their financial support.

SUPPLEMENTARY MATERIAL

The Supplementary Material for this paper is available online at https://dx.doi.org/10.2166/wst.2020.150.

REFERENCES

Ali, B., ur-Rehman, A., Ghafoor, F., Shahzad, M. I., Shah, S. K. & Abbas, S. M. 2018 Interconnected mesoporous Na_2FeSiO_4 nanospheres supported on carbon nanotubes as a highly stable and efficient cathode material for sodium-ion battery. *Journal of Power Sources* **396**, 467–475.

Barhoumi, N., Oturan, N., Olvera-Vargas, H., Brillas, E., Gadri, A., Ammar, S. & Oturan, M. A. 2016 Pyrite as a sustainable catalyst in electro-Fenton process for improving oxidation of sulfamethazine. Kinetics, mechanism and toxicity assessment. *Water Research* **94**, 52–61.

Chen, J. & Zhu, L. 2009 Comparative study of catalytic activity of different Fe-pillared bentonites in the presence of UV light and H_2O_2. *Separation and Purification Technology* **67** (3), 282–288.

Chen, J. & Zhu, L. 2011 Oxalate enhanced mechanism of hydroxyl-Fe-pillared bentonite during the degradation of Orange II by UV-Fenton process. *Journal of Hazardous Materials* **185** (2), 1477–1481.

Chen, L., Deng, C., Wu, F. & Deng, N. 2011 Decolorization of the azo dye Orange II in a montmorillonite/H_2O_2 system. *Desalination* **281**, 306–311.

Chen, M., Peng, K., Wang, H., Yang, Z., Zeng, Q. & Xu, A. 2012 High performance of a simple cobalt(II)–monoethanolamine complex for orange II degradation with H_2O_2 as an oxidant at ambient conditions. *Chemical Engineering Journal* **197** (14), 110–115.

Dai, H., Xu, S., Chen, J., Miao, X. & Zhu, J. 2018 Oxalate enhanced degradation of Orange II in heterogeneous UV-Fenton system catalyzed by Fe_3O_4@γ-Fe_2O_3 composite. *Chemosphere* **199**, 147–153.

De La Cruz, N., Giménez, J., Esplugas, S., Grandjean, D., de Alencastro, L. F. & Pulgarín, C. 2012 Degradation of 32 emergent contaminants by UV and neutral photo-Fenton in domestic wastewater effluent previously treated by activated sludge. *Water Research* **46** (6), 1947–1957.

do Nascimento, G. E., Napoleão, D. C., da Rocha Santana, R. M., Charamba, L. V. C., de Oliveira, J. G. C., de Moura, M. C., Coelho, L. C. B. B. & Duarte, M. M. M. B. 2018 Degradation of textile dyes Remazol Yellow Gold and reactive Turquoise: optimization, toxicity and modeling by artificial neural networks. *Water Science and Technology* **2017** (3), 812–823.

Fu, Y., Yu, S. L., Yy, Y. Z., Qiu, L. P. & Hui, B. 2007 Reaction mode between Si and Fe and evaluation of optimal species in poly-silicic-ferric coagulant. *Journal of Environmental Sciences* **19** (6), 678–688.

Fu, Y., Yu, S. & Han, C. 2009 Morphology and coagulation performance during preparation of poly-silicic-ferric (PSF) coagulant. *Chemical Engineering Journal* **149**, 1–10.

Guo, S., Zhang, G. & Wang, J. 2014 Photo-Fenton degradation of rhodamine B using Fe_2O_3–Kaolin as heterogeneous catalyst: characterization, process optimization and mechanism. *Journal of Colloid and Interface Science* **433** (11), 1–8.

Guo, S., Zhang, G. & Yu, J. C. 2015 Enhanced photo-Fenton degradation of rhodamine B using graphene oxide–amorphous $FePO_4$ as effective and stable heterogeneous catalyst. *Journal of Colloid and Interface Science* **448**, 460–466.

Huang, M., Zhou, T., Wu, X. & Mao, J. 2017 Distinguishing homogeneous-heterogeneous degradation of norfloxacin in a photochemical Fenton-like system (Fe_3O_4/UV/oxalate) and the interfacial reaction mechanism. *Water Research* **119**, 47–56.

Kakavandi, B., Takdastan, A., Jaafarzadeh, N., Azizi, M., Mirzaei, A. & Azari, A. 2016 Application of Fe_3O_4@C catalyzing heterogeneous UV-Fenton system for tetracycline removal with a focus on optimization by a response surface method. *Journal of Photochemistry and Photobiology A: Chemistry* **314** (1), 178–188.

Karci, A., Arslan-Alaton, I. & Bekbolet, M. 2013 Oxidation of nonylphenol ethoxylates in aqueous solution by UV-C photolysis, H_2O_2/UV-C, Fenton and photo-Fenton processes: are these processes toxicologically safe? *Water Science and Technology* **68** (8), 1801–1809.

Leifeld, V., Santos, T. P. M. D., Zelinski, D. W. & Igarashi-Mafra, L. 2018 Ferrous ions reused as catalysts in Fenton-like reactions for remediation of agro-food industrial wastewater. *Journal of Environmental Management* **222**, 284–292.

Lenoble, V., Laclautre, C., Deluchat, V., Serpaud, B. & Bollinger, J. C. 2005 Arsenic removal by adsorption on iron(III) phosphate. *Journal of Hazardous Materials* **123** (1), 262–268.

Li, J., Liu, X. & Cheng, F. 2017 Bio-refractory organics removal and floc characteristics of poly-silicic-cation coagulants in tertiary-treatment of coking wastewater. *Chemical Engineering Journal* **324**, 10–18.

Li, J., Li, J., Liu, X., Du, Z. & Cheng, F. 2018 Effect of silicon content on preparation and coagulation performance of poly-silicic-metal coagulants derived from coal gangue for coking wastewater treatment. *Separation and Purification Technology* **202**, 149–156.

Li, Y., Chen, D., Fan, S. & Yang, T. 2019 Enhanced visible light assisted Fenton-like degradation of dye via metal-doped zinc ferrite nanosphere prepared from metal-rich industrial wastewater. *Journal of the Taiwan Institute of Chemical Engineers* **96**, 185–192.

Liu, L., Wu, C., Chen, Y. & Wang, H. 2017 Preparation, characterization and coagulation behaviour of polyferric magnesium silicate (PFMSi) coagulant. *Water Science and Technology* **75** (8), 1961–1970.

Miao, X., Dai, H., Chen, J. & Zhu, J. 2018 The enhanced method of hydroxyl radical generation in the heterogeneous UV-Fenton system with α-FeOOH as catalyst. *Separation and Purification Technology* **200**, 36–43.

Moon, B. H., Park, Y. B. & Park, K. H. 2011 Fenton oxidation of Orange II by pre-reduction using nanoscale zero-valent iron. *Desalination* **268** (1), 249–252.

Paz, E. C., Aveiro, L. R., Pinheiro, V. S., Souza, F. M., Lima, V. B., Silva, F. L., Hammer, P., Lanza, M. R. V. & Santos, M. C. 2018 Evaluation of H_2O_2 electrogeneration and decolorization of Orange II Azo Dye using tungsten oxide nanoparticle-modified carbon. *Applied Catalysis B: Environmental* **232**, 436–445.

Qian, X., Ren, M., Zhu, Y., Yue, D., Han, Y., Jia, J. & Zhao, Y. 2017 Visible light assisted heterogeneous Fenton-like degradation of organic pollutant via α-FeOOH/Mesoporous carbon composites. *Environmental Science and Technology* **51** (7), 3993–4000.

Rosari, S. & Ardiansyah, T. 2019 Degradation of methylene blue and Congo-red dyes using Fenton, photo-Fenton, sono-Fenton, and sonophoto-Fenton methods in the presence of iron(II,III) oxide/zinc oxide/graphene (Fe_3O_4/ZnO/graphene) composites. *Separation and Purification Technology* **210**, 563–573.

Shuai, W., Liu, C., Fang, G., Zhou, D. & Gao, J. 2018 Nano-α-Fe_2O_3 enhanced photocatalytic degradation of diethyl phthalate ester by citric acid/UV (300–400 nm): a mechanism study. *Journal of Photochemistry and Photobiology A: Chemistry* **360**, 78–85.

Su, S., Cao, C., Zhao, Y. & Dionysiou, D. D. 2019 Efficient transformation and elimination of roxarsone and its metabolites by a new α-FeOOH@GCA activating persulfate system under UV irradiation with subsequent As(V) recovery. *Applied Catalysis B: Environmental* **245**, 207–219.

Sun, T., Liu, L. L., Wan, L. L. & Zhang, Y. P. 2010 Effect of silicon dose on preparation and coagulation performance of poly-ferric-aluminum-silicate-sulfate from oil shale ash. *Chemical Engineering Journal* **163** (1), 48–54.

Sun, T., Sun, C. H., Zhu, G. L., Miao, X. J., Wu, C. C., Lv, S. B. & Li, W. J. 2011 Preparation and coagulation performance of poly-ferric-aluminum-silicate-sulfate from fly ash. *Desalination* **268** (1), 270–275.

Tan, C., Dong, Y., Shi, L., Chen, Q., Yang, S., Liu, X., Ling, J., He, X. & Fu, D. 2018 Degradation of Orange II in ferrous activated peroxymonosulfate system: efficiency, situ EPR spin trapping and degradation pathway study. *Journal of the Taiwan Institute of Chemical Engineers* **83**, 74–81.

Xu, S. Y., Chen, J. X., Wang, L., Jiang, B. Q. & Gong, X. 2017 Catalytic features of iron oxides with different crystal forms during Orange II degradation in Fenton and UV-Fenton systems. *Journal of Safety & Environment* **17** (4), 1448–1453.

Wang, Y., Sun, Y., Li, W., Tian, W. & Irini, A. 2015 High performance of nanoscaled Fe_2O_3 catalyzing UV-Fenton under neutral condition with a low stoichiometry of H_2O_2 : kinetic study and mechanism. *Chemical Engineering Journal* **267**, 1–8.

Wang, Y., Lin, X., Shao, Z., Shan, D., Li, G. & Irini, A. 2016 Comparison of Fenton, UV-Fenton and Nano-Fe_3O_4 catalyzed UV-Fenton in degradation of phloroglucinol under neutral and alkaline conditions: role of complexation of Fe^{3+} with hydroxyl group in phloroglucinol. *Chemical Engineering Journal* **313**, 938–945.

Yang, X., Yang, Z., Liu, Z., Zhang, W. & Wang, D. 2018 Enhanced mineralization of hypersaline wastewater with Fe^{2+}/Cu^{2+} catalyzed UV-Fenton process: process optimization and catalytic mechanism. *Water Science and Technology* **78** (5), 1219–1227.

Ying, X. S., Chen, J. X., Wang, L., Jiang, B. Q. & Gong, X. 2017 Catalytic features of iron oxides with different crystal forms during Orange II degradation in Fenton and UV-Fenton systems. *Journal of Safety & Environment* **17** (4), 1448–1453.

Yu, L., Chen, J., Liang, Z., Xu, W., Chen, L. & Ye, D. 2016 Degradation of phenol using Fe_3O_4-GO nanocomposite as a heterogeneous photo-Fenton catalyst. *Separation and Purification Technology* **171**, 80–87.

Zhang, Q., Yan, C., Dai, Q. & Su, C. 2017 Facile synthesis and lithium storage properties of engineered ultrafine porous Fe_2SiO_4/C composites. *Journal of Electroanalytical Chemistry* **807**, 29–36.

Zulfiqar, M., Sujan, C., Suriati, S. & Omar, A. A. 2018 Enhanced photocatalytic activity of Orange II in aqueous solution using solvent-based TiO_2 nanotubes: kinetic, equilibrium and thermodynamic studies. *Journal of Cleaner Production* **203**, 848–859.

First received 12 July 2019; accepted in revised form 23 March 2020. Available online 2 April 2020